An image hiding scheme in a 2-dimensional coupled map lattice of matrices

Guangqing Lu[a], Rasa Smidtaite[b, c], Daniel Howard[d], Minvydas Ragulskis[a, b, *]

[a] School of Electrical and Information Engineering of Jinan University, 206 Qianshan Road, Zhuhai, 519070, Guangdong, PR China
[b] Center for Nonlinear Systems, Kaunas University of Technology, Studentu 50–146, Kaunas LT-51368, Lithuania
[c] Department of Applied Mathematics, Kaunas University of Technology, Studentu 50–318, Kaunas LT-51368, Lithuania
[d] Howard Science Limited, Malwern, U.K.

ARTICLE INFO

Keywords:
Coupled map lattice
Nilpotent matrix
Spatiotemporal chaos
Image hiding

ABSTRACT

An image hiding scheme in a 2-dimensional coupled map lattice of matrices is presented in this paper. Scalar variables at each node of the lattice are replaced by nilpotent matrices. The spatiotemporal divergence process is employed to hide the secret digital image in the state map of the nodal variables. The presented image hiding scheme does not require the computation of the difference image between two patterns produced by the perturbed and the unperturbed initial conditions. Computational experiments are used to demonstrate the efficacy of the presented technique.

1. Introduction

Coupled map lattices (CML) play an important role in the study of the chaotic dynamics of spatially extended systems. A CML generally incorporates a finite number of coupled nodes. The major difference of a CML from a cellular automata network is that each node of the CML is dependent upon its neighbors relative to the coupling term in the recurrence equation [1]. CMLs have been used to generate, illustrate and describe such complex phenomena as spatial bifurcations, frozen chaos, spatio-temporal intermittency, global travelling waves [2–4].

Scalar variables at each node of the CML can be replaced by matrix variables [5]. It is shown in [5] that such models of CMLs of matrices (CMLM) can diverge if initial nodal matrices are nilpotent matrices. Moreover, such CMLMs can generate fractal patterns representing spatiotemporal divergence that can be controlled by the coupling parameter between the nodes [5].

Self-organization is a process where some form of order arises from interactions between parts of initially disordered systems. Self-organization occurs in a variety of physical (granular material, liquid crystals), biological (growth of colonies, animal markings), chemical systems (Turing patterns, reaction-diffusion systems) [6–8]. Self-organizing patterns are widely exploited in computer science and informatics – particularly for hiding and communicating secret visual images. A fingerprint is used as the initial condition for the evolution of a self-organizing pattern in a network of cellular automata with elements representing the reaction-diffusion processes [9]. Beddington–DeAngelis type predator-prey model with self- and cross-diffusion is exploited in a steganographic digital image communication system developed in [10,11]. Spatial 2×2 games, atrial fibrillation models, non-diffusively coupled nonlinear maps, breaking spiral waves are used to generate self-organizing patterns and to hide and to communicate a secret digital image [12–15].

An alternative digital image hiding technique based on Abelian sandpiles is proposed in [16]. Perturbations of the digital image are self-erased in this scheme. That allows to heal the corrupted image (if only the cover image is encoded into the sandpile attractor). On the contrary, image hiding schemes based on self-organizing patterns do not self-erase perturbations. Perturbations are amplified and do propagate throughout the domain due to the nonlinear evolution of the pattern [12–15].

The features, operation principles, the information capacity of communication schemes based on self-organizing patterns are all different. The "No-free-lunch theorem" [17] implies that every particular communication scheme does possess some or another sort of deficiencies. For example, the scheme based on Beddington–DeAngelis model is computationally ineffective and requires at least 10 000 time-forward integration steps of a system of nonlinear partial differential equations [10]. The scheme based on spatial

* Corresponding author.
E-mail address: minvydas.ragulskis@ktu.lt (M. Ragulskis).

2×2 games is not sensitive to local perturbations of an individual pixel [13]. The information capacity of a scheme based on non-diffusively coupled nonlinear maps is comparatively low [14]. The scheme based on breaking spiral waves requires an iterative correction of individual perturbations of pixels [15].

However, a general feature of all discussed communication schemes (based on self-organizing patterns) is based on the computational processing of the difference image which is computed as the XOR difference between a pattern produced by the perturbed and non-perturbed initial conditions. The objective of this paper is to exploit the effect of the spatiotemporal divergence produced by a CMLM in such a way that the interpretation of the secret image would not require the difference image.

2. Preliminaries and the motivation

2.1. The simplified nilpotent model of the logistic coupled map lattice of matrices

The classical Kaneko model of Coupled Map Lattices (CML) with periodic boundary conditions [18] is a paradigmatic model representing the complex dynamics of spatiotemporal chaos:

$$x^{(t+1)}(i) = (1-\varepsilon) f\left(x^{(t)}(i)\right) + \frac{\varepsilon}{2}\left(f\left(x^{(t)}(i+1)\right) + f\left(x^{(t)}(i-1)\right)\right) \tag{1}$$

where t is a discrete time step; i is the nodal point of the lattice ($i = 1, 2, \ldots, N$, N is the size of the CML); ε is the coupling parameter, $f(x)$ is a scalar mapping function (usually set as the Logistic mapping function: $f(x) = ax(1-x)$; $0 \le a \le 4$ [19]). Properties of such CML are very well explored; the applications ranging from complex network dynamics to computational biology [20–23].

As stated previously, the main objective of this paper is to study a 2D CML where scalar nodal variables $x^{(t)}(i)$ are replaced by matrix variables $\mathbf{X}^{(t)}(i) \in \mathbb{R}^{2\times 2}$. However, the dynamics of a 1D CML where scalar nodal variables $x^{(t)}(i)$ are replaced by matrix variables $\mathbf{X}^{(t)}(i) \in \mathbb{R}^{2\times 2}$ is already studied in [5]. It is demonstrated in [5] that a 1D coupled map lattice of matrices (CMLM) can diverge when all initial matrices are nilpotent matrices. This effect served as a motivation to design a simplified nilpotent model of a 1D CMLM [5]:

$$\begin{cases} \lambda_0^{(t+1)}(i) = a(i)\lambda_0^{(t)}(i)\left(1-\lambda_0^{(t)}(i)\right); \\ \mu^{(t+1)}(i) = (1-\varepsilon)a(i)\mu^{(t)}(i)\left(1-2\lambda_0^{(t)}(i)\right) \\ \quad +\frac{\varepsilon}{2}\left(a(i+1)\mu^{(t)}(i+1)\left(1-2\lambda_0^{(t)}(i+1)\right)\right. \\ \quad \left.+a(i-1)\mu^{(t)}(i-1)\left(1-2\lambda_0^{(t)}(i-1)\right)\right); \end{cases} \tag{2}$$

where t is discrete time ($t = 0, 1, 2, \ldots$); i is the number of the node ($i = 1, 2, \ldots, N$); $0 \le \lambda_0^{(0)}(i) \le 1$ is the Eigenvalue of the initial nilpotent matrix at node i; $\mu^{(0)}(i) = 1$ is the nilpotent parameter of the initial nilpotent matrix at node i; and $a(i)$ is the parameter of the Logistic map at node i. In other words, the simplified nilpotent model of a 1D CMLM mimics the evolution of an isolated Logistic map of matrices with a nilpotent initial matrix – except that the nilpotent parameters $\mu^{(t)}(i)$ are linked by the Kaneko model [5]. Note that the parameters of the Logistic map $a(i)$ can be different at different nodes. The simplified nilpotent model of CMLM comprises two scalar maps – therefore the lattice parameters $\lambda_0^{(t)}(i)$ and $\mu^{(t)}(i)$ are computed directly instead of performing matrix computations on the lattice.

Clearly, the first equation of the 1D CMLM represents an array of uncoupled Logistic maps. The second equation of the 1D CMLM interlinks Eigenvalues and nilpotent parameters of adjacent nodes. It is demonstrated in [5] that $\mu^{(t)}(i)$ can diverge when the parameters of the Logistic map $a(i)$ are set to the values corresponding to the chaotic evolution of the scalar Logistic map [5].

2.2. The simplified nilpotent model of a 2D CMLM

Let us consider a natural 2D extension of the simplified nilpotent model of a 1D CMLM with 4 neighbors on a rectangular domain $[1; N_x] \times [1; N_y]$ with periodic boundary conditions (N_x and N_y denotes the number of pixels in x and y directions respectively):

$$\begin{cases} \lambda_0^{(t+1)}(i,j) = a(i,j)\lambda_0^{(t)}(i,j)\left(1-\lambda_0^{(t)}(i,j)\right); \\ \mu^{(t+1)}(i,j) = (1-\varepsilon)a(i,j)\mu^{(t)}(i,j)\left(1-2\lambda_0^{(t)}(i,j)\right) \\ \quad +\frac{\varepsilon}{4}\left(a(i+1,j)\mu^{(t)}(i+1,j)\left(1-2\lambda_0^{(t)}(i+1,j)\right)\right. \\ \quad +a(i-1,j)\mu^{(t)}(i-1,j)\left(1-2\lambda_0^{(t)}(i-1,j)\right) \\ \quad +a(i,j+1)\mu^{(t)}(i,j+1)\left(1-2\lambda_0^{(t)}(i,j+1)\right) \\ \quad \left.+a(i,j-1)\mu^{(t)}(i,j-1)\left(1-2\lambda_0^{(t)}(i,j-1)\right)\right) \end{cases} \tag{3}$$

where indexes (i, j) denote the coordinates of a pixel; $\mu^{(0)}(i,j) = 1$; $0 \le \lambda_0^{(0)}(i,j) \le 1$; $0 \le a(i,j) \le 4$; $i = 1, 2, \ldots, N_x$; $j = 1, 2, \ldots, N_y$.

2.3. The motivation for the construction of the 2D CMLM

Clearly, the simplified nilpotent model of a 2D CMLM does inherit such properties of the 1D model as the divergence of the nilpotent parameters. However, the main objective of this paper goes further than the simple exploration of the dynamical properties of the 2D model. The main objective of this study is to develop such an image hiding scheme which would not require a difference image for the retrieval of the secret image. A computational procedure for the image hiding scheme based on the difference between two self-organizing patterns can be illustrated by the following scheme [10,15]:

Part 1. Encoding a secret image into a self-organizing pattern (the actions of the Sender):

1. Generate a random grayscale image on the rectangular grid $[1; N_x] \times [1; N_y]$.
2. Perturb the generated random image at several pre-selected pixels (the dot skeleton representation of the secret image). The perturbation is lower than the noise level of the random image.
3. Use the perturbed random image as the initial conditions for the algorithm generating a self-organizing pattern.
4. Use the generated pattern as the cover image. Send the cover image to the Receiver.

Part 2. Decoding the secret image (the actions of the Receiver):

1. Retrieve the parameters of the algorithm generating a self-organizing pattern (private and public keys).
2. Generate the random grayscale image on the rectangular grid $[1; N_x] \times [1; N_y]$ (identical random image to the one used in the encoding stage).
3. Use the unperturbed random image as the initial conditions for the algorithm generating a self-organizing pattern.
4. Receive the cover image from the Sender.
5. Compute the difference between the generated self-organizing pattern and the cover image. The difference image reveals the secret image.

The objective of this paper is to propose such an image hiding scheme which does not require the computation of the difference image.

3. The construction of the image hiding scheme

3.1. The perturbation of a single pixel

The initial Eigenvalues $\lambda_0^{(0)}(i,j)$ in Eq. (3) can be randomly distributed in interval [0, 1] – but all nilpotent parameters $\mu^{(0)}(i,j)$

must be set to 1 (this is required by the structure of the simplified nilpotent model of a CMLM [5]). The perturbation of a single pixel at coordinates $(k,\ l)$ at $t = 0$ will be considered in this section. Two options are available – the perturbation of $\lambda_0^{(0)}(k, l)$ or $a(k,\ l)$.

3.1.1. The perturbation of $\lambda_0^{(0)}(k, l)$

Let us consider a rectangular grid $[1;\ 40] \times [1;\ 40]$ with a single pixel to be perturbed at $k = 20;\ l = 20$. Let all parameters of the Logistic map $a(i,\ j)$ be set to 3.565 (the onset of chaos for the scalar Logistic map). A pseudorandom number generator can be used to set the initial distribution of $\lambda_0^{(0)}(i,\ j)$. A simple scalar Logistic map can be used for that purpose – but we use the intertwining Logistic map [24] in order to avoid such drawbacks of the standard Logistic map as a limited uniformity of generated values, stable windows and relatively small space of valid seeds [25].

The perturbation is performed according to the following rule:

$$\widetilde{\lambda}_0^{(0)}(k, l) = \begin{cases} \lambda_0^{(0)}(k, l) + 0.1 & \text{if } \lambda_0^{(0)}(k, l) \le 0.5 \\ \lambda_0^{(0)}(k, l) - 0.1 & \text{if } \lambda_0^{(0)}(k, l) > 0.5 \end{cases}$$

The resulting image of $\mu^{(200)}(i,\ j)$ produced by the 2D CMLM does not reveal the divergence. Some changes around $k = 20;\ l = 20$ can be seen in the difference image between the patterns produced by the perturbed and non-perturbed initial conditions (Fig. 1). However, such image hiding technique does not possess any principal advantages over the previously reported schemes [10,15] and will not be further considered.

Computational experiments are continued with the perturbation of $\lambda_0^{(0)}(k, l)$ – but all parameters $a(i,\ j)$ are now set to $a = 3.59$. The 2D CMLM diverges both from the perturbed and non-perturbed initial conditions (Fig. 2). Moreover, the difference image does not reveal anything if cropping is used for the visualization of $\mu^{(200)}(i,\ j)$ (Fig. 2).

3.1.2. The perturbation of a(k, l)

The intertwining Logistic map is used to generate the initial random distribution of $\lambda_0^{(0)}(i,\ j)$ in interval [0,1]; initial parameters $\mu^{(0)}(i,\ j)$ are set to 1; $i,\ j = 1, 2, \ldots, 40$. All parameters $a(i,\ j)$ are set to 3.565 except one pixel at coordinates (20, 20). The perturbation magnitude is $\Delta a = 0.025;\ a(20, 20) = 3.590$. Such perturbation brings the node (20, 20) into the chaotic state what results into the divergence [5]. Moreover, complex interactions between adjacent nodes results into complex transient behavior of the 2D CMLM (Fig. 3).

It is shown in [5] that the coupling parameter ε between nodes can control the process of divergence in 1D CMLM. A similar process is observed in the 2D CMLM (Fig. 3). Initially, ε is set to 0.05. The states of all nodes after 200 time-forward iterations is shown in Fig. 3(a). Note that numerical values of $\mu^{(200)}(i,\ j)$ greater than 5 are truncated to 5 for the clarity of visual representation (the trun-

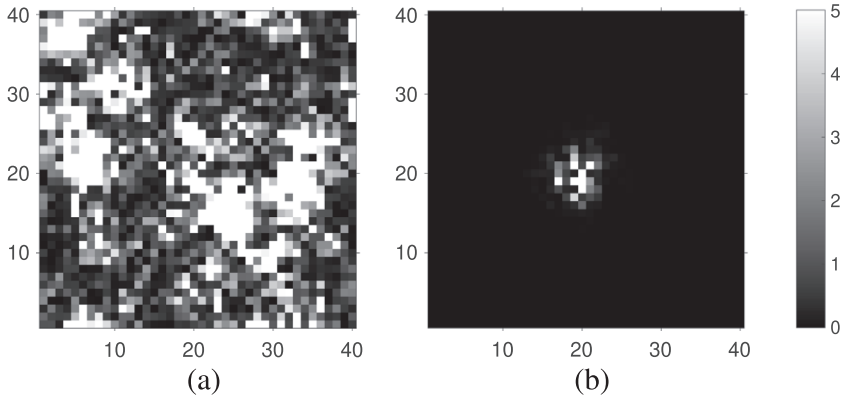

Fig. 1. The perturbation of $\lambda_0^{(0)}(20, 20)$ yields an interpretable response only in the difference image. The state map of nodal parameters $\mu^{(t)}(i,\ j)$ after 200 time-forward iterations is shown in part a (the grid size is 40×40 nodes with periodic boundary conditions). Parameters $\lambda_0^{(0)}(i,\ j)$ are randomly distributed in interval [0,1]; $\mu^0(i,\ j) = 1;$ $i,\ j = 1, 2, \ldots, 40$. All parameters $a(i,\ j)$ are set to 3.565; the coupling parameter ε is set to 0.08. The difference image between the pattern of $\mu^{(t)}(i,\ j)$ produced by the perturbed and the nonperturbed initial conditions after 200 time-forward iterations is shown in part b.

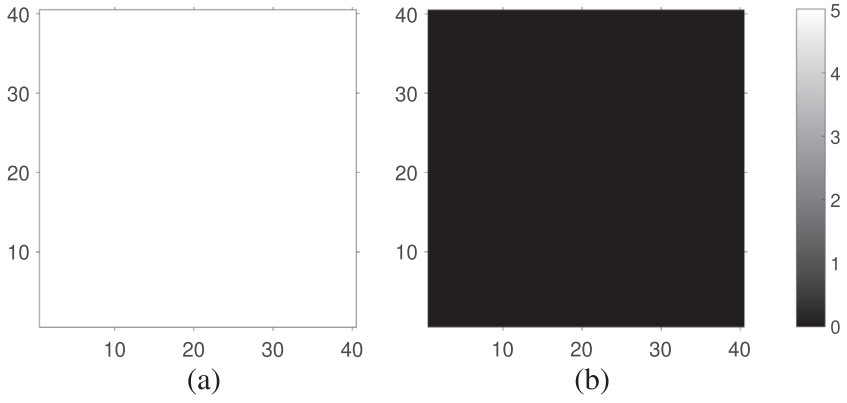

Fig. 2. The perturbation of $\lambda_0^{(0)}(20, 20)$ does not yield any interpretable response when the 2D CMLM diverges. The state map of nodal parameters $\mu^{(t)}(i,\ j)$ after 200 time-forward iterations is shown in part a (the grid size is 40×40 nodes with periodic boundary conditions). Parameters $\lambda_0^{(0)}(i,\ j)$ are randomly distributed in interval [0,1]; $\mu^{(0)}(i,\ j) = 1;\ i,\ j = 1, 2, \ldots, 40$. All parameters $a(i,\ j)$ are set to 3.59; the coupling parameter ε is set to 0.08. The difference image between the pattern of $\mu^{(t)}(i,\ j)$ produced by the perturbed and the nonperturbed initial conditions after 200 time-forward iterations is shown in part b.

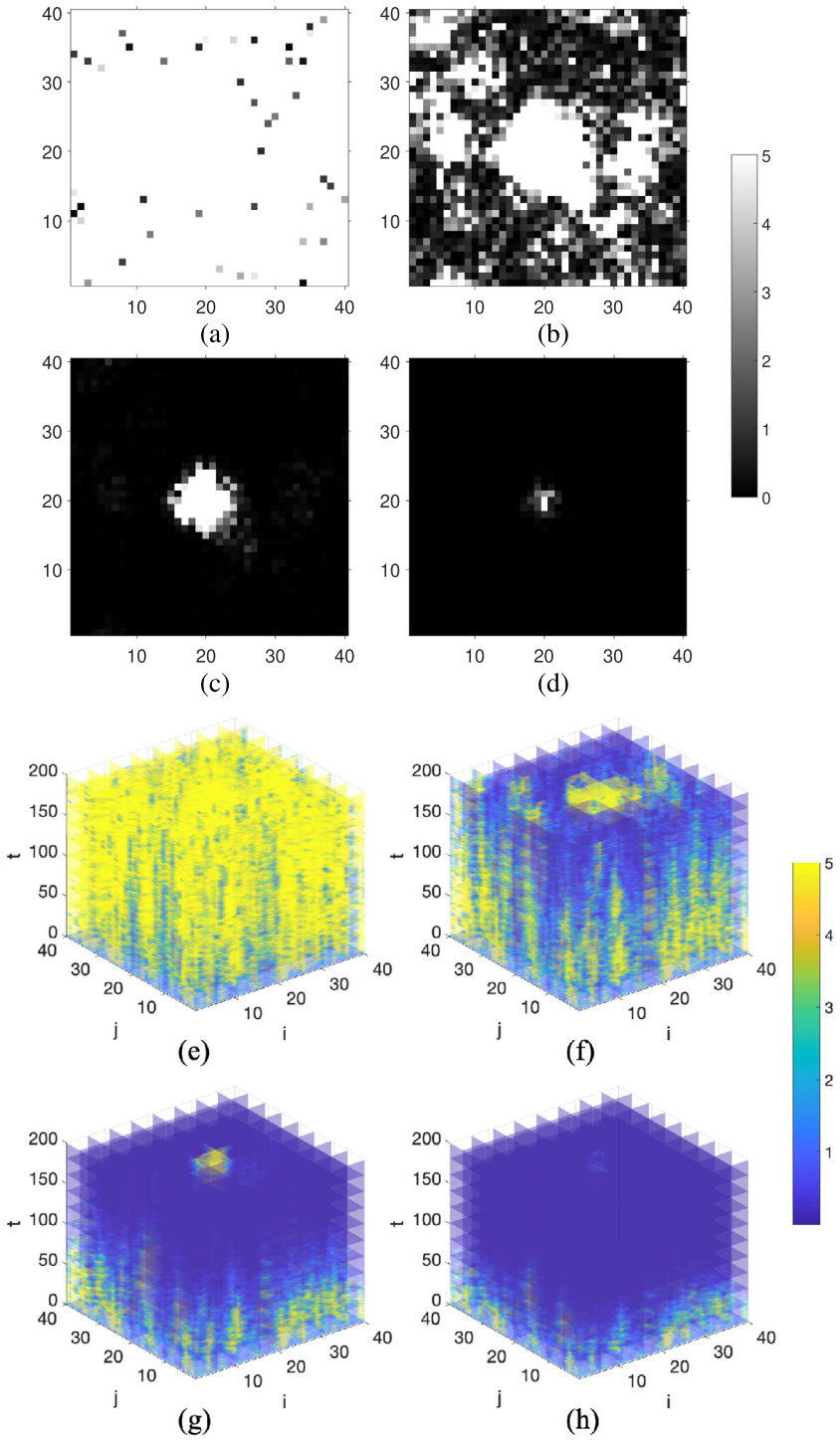

Fig. 3. The coupling parameter ε can suppress the divergence of the simplified nilpotent model of the 2D CMLM in 200 time-forward iterations (the grid size is 40×40 nodes with periodic boundary conditions). Parameters $\lambda_0^{(0)}(i,j)$ are randomly distributed in interval [0, 1]; $\mu^{(0)}(i,j) = 1$; $i, j = 1, 2, \ldots, 40$. All parameters $a(i,j)$ are set to 3.565 except one pixel at coordinates (20, 20). The perturbation magnitude is $\Delta a = 0.025$; $a(20,20) = 3.590$. The coupling parameter ε is set to 0.05 in parts (a) and (e); $\varepsilon = 0.08$ in parts (b) and (f); $\varepsilon = 0.11$ in parts (c) and (g); $\varepsilon = 0.15$ in parts (d) and (h).

cation does not affect the computational evolution of the model). It appears that the perturbation of 1 single pixel did excite the whole network; $\mu^{(200)}(i,j) = 6.77 \cdot 10^7$. Transient processes are shown in Fig. 3(e); eight semi-transparent section planes are constructed in both directions in order to visualize the complexity of transitions.

Larger values of the coupling parameter ε do suppress the divergence. The states of all nodes after 200 time-forward iterations and the transient processes at $\varepsilon = 0.08$ are shown in Fig. 3 parts b and f $\left(\mu^{(200)}(i,j) = 7.96 \cdot 10^6\right)$; $\varepsilon = 0.11$ – Fig. 3 parts c and g $\left(\mu^{(200)}(i,j) = 1.82 \cdot 10^3\right)$; $\varepsilon = 0.15$ – Fig. 3 parts d and h $\left(\mu^{(200)}(i,j) = 0.59\right)$.

It is clear that the transient processes in a 2D CMLM are predetermined not only by the coupling parameter ε but also by the perturbation magnitude Δa. We continue with the computational setup used in Fig. 3 – but fix ε to 0.11 and vary the magnitude of the perturbation Δa at the node (20, 20) (Fig. 4). The states of

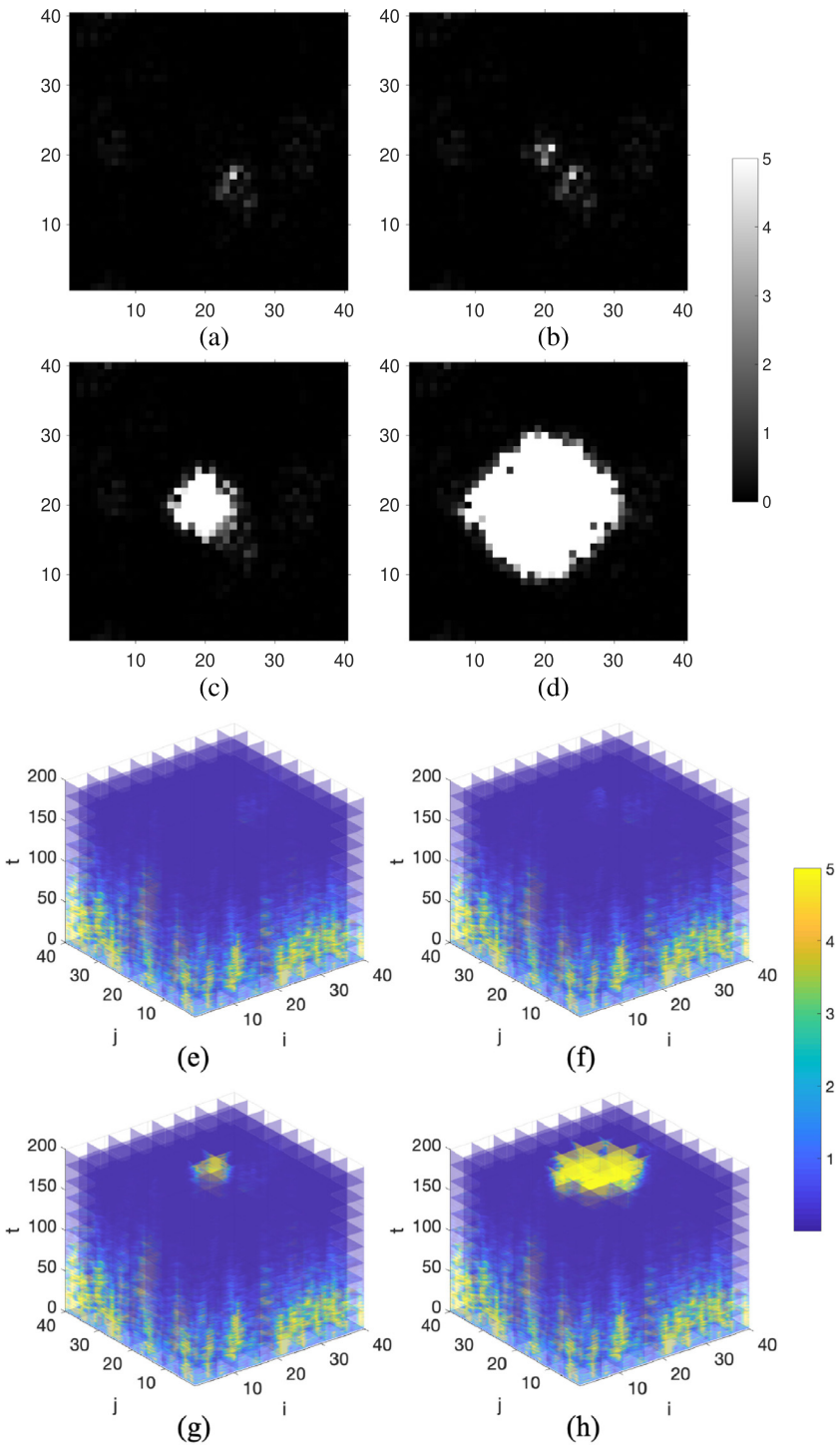

Fig. 4. The perturbation Δa defines the size and the shape of the set of diverged nodes in the simplified nilpotent model of the 2D CMLM in 200 time-forward iterations (the grid size is 40×40 nodes with periodic boundary conditions). Parameters $\lambda_0^{(0)}(i, j)$ are randomly distributed in interval [0, 1]; $\mu^{(0)}(i, j) = 1$; $i, j = 1, 2, \ldots, 40$; the coupling parameter ε is set to 0.11. All parameters $a(i, j)$ are set to 3.565 except one pixel at coordinates (20, 20). The perturbation magnitude $\Delta a = 0.005$ in parts (a) and (e); $\Delta a = 0.01$ in parts (b) and (f); $\Delta a = 0.025$ in parts (c) and (g); $\Delta a = 0.055$ in parts (d) and (h).

all nodes after 200 time-forward iterations are shown in Fig. 4(a); numerical values of $\mu^{(200)}(i, j)$ greater than 5 are truncated to 5 for clarity. It is interesting to note that the perturbation of the central pixel does result into the response of a group of pixels not centered around the central pixel (Fig. 4(a)). That can be explained by complex transient processes taking place in the evolution of the 2D CMLM. The larger is the magnitude of the perturbation Δa, the more violent is the reaction of the 2D CMLM after 200 time-forward iterations (Fig. 4 parts b and f, c and g, d and h).

3.2. The perturbation of 2 separate pixels

The ability to form and to control a distinctive shape in the state map of the 2D CMLM is an important feature which builds a foundation for the construction of a digital image communication

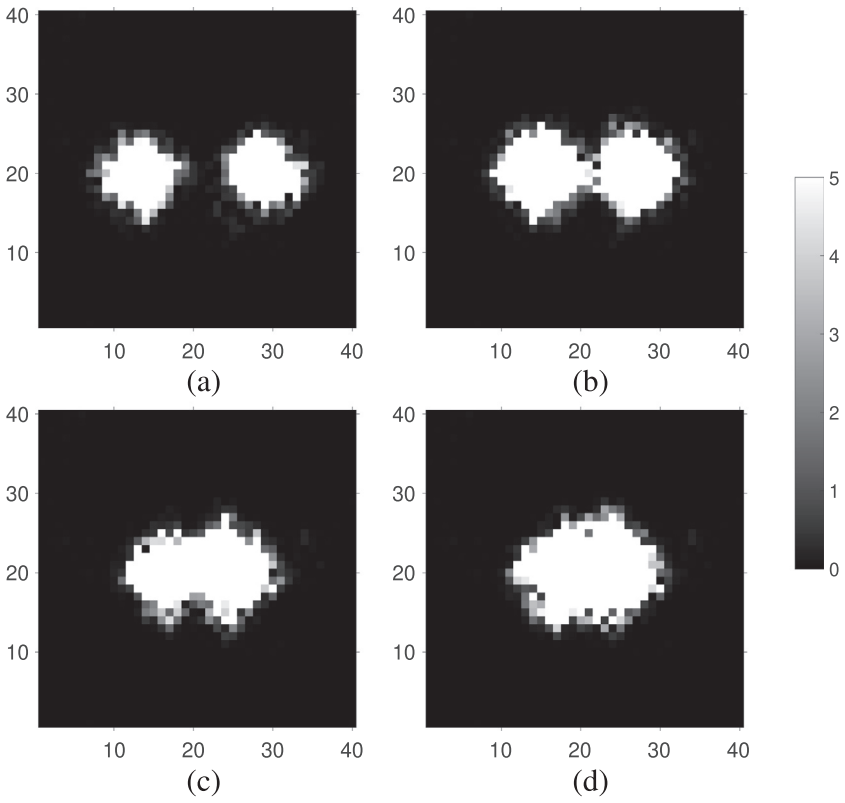

Fig. 5. Evolution of Simplified Nilpotent Model of 2D CMLM after 180 iterations when two pixels are perturbated (the whole domain is 40×40). Parameters are $a(i, j) = 3.565,\ \Delta a = 0.03, \varepsilon = 0.13$. The clearance between two skeleton dots is (a) 15 pixels; (b) 11 pixels; (c) 6 pixels; (d) 4 pixels.

algorithm. However, the information capacity is an important feature of such an algorithm. In other words, it is necessary to determine the minimal distance between two perturbation points which results into interpretable and separable shapes in the state map of the 2D CMLM.

Computational experiments are continued with the same setup of the 2D CMLM. The coupling parameter ε is set to 0.13; the perturbation magnitude Δa is set to 0.03. The distance between the two perturbed points is gradually reduced – until the shapes induced by the two perturbed points are inseparable in the state map after 180 time-forward iterations (Fig. 5).

The proposed scheme is based on digital image hiding in self-organizing patterns. It is natural to expect that the information capacity of this scheme is comparable to other image hiding schemes based on self-organizing patterns [10,14] and cannot compete to steganographic schemes. The smallest element of the image in the proposed scheme is not a pixel. It is a recognizable and an interpretable element in the evolved pattern after a predetermined number of time-forward steps.

All perturbations of the initial conditions (at pixels corresponding to the dot-skeleton representation of the secret image) are comparable to the noise level governing the random distribution of pixels. Moreover, these perturbations can be both positive and negative. The principal difference between the proposed scheme and any steganographic scheme is based on the fact that the cover image simply does not exist. There is nothing what can be compared (the cover image and the perturbed image). One needs to run the algorithm governing the evolution of the self-organizing system until the pattern is clearly interpretable.

It is natural to expect that such a useful functionality does not occur without any sacrifices (as pre-determined by the No-free-lunch theorem [17]). The information capacity of the proposed scheme (the minimum distance between pixels in the dot-skeleton representation of the secret image) is 11 pixels (Fig. 5). As mentioned previously, this is comparable to other image hiding schemes based on self-organizing patterns (but based on difference images).

4. An image hiding algorithm based on the 2D CMLM

The schematic diagram of the image communication algorithm based on the 2D CMLM is depicted in Fig. 6. Initially, the original image is transformed into its dot-skeleton representation [10] (the density of dots is predefined by the information capacity of the algorithm). Then, parameters $a(i, j)$ are set to a value corresponding to the onset of chaos of the Logistic map – and are perturbed at pixels corresponding to the dot-skeleton representation of the original image. The magnitude of perturbation Δa is an integral parameter of the algorithm; the symbol [**1**] denotes the matrix of ones (Fig. 6).

Next, all initial parameters $\mu^{(0)}(i, j)$ are set to 1. A random number generator is used to generate the initial random distribution of $\lambda_0^{(0)}(i, j)$ in interval [0, 1]. The scalar iterative function $f(x)$ (the Logistic map) is used to iterate $\lambda_0^{(t)}(i, j)$ (the first iterative relationship in Eq. (3)). The 2D CMLM is used to iterate $\mu^{(t)}(i, j)$ (Fig. 6). The stopping criterion (the number of time-forward steps) is an integral parameter of the algorithm. Numerical values of $\mu^{(t)}(i, j)$ are truncated to 5 – the resulting plot of $\mu^{(t)}(i, j)$ reveals the approximation of the original image (Fig. 6).

It is completely natural that the parameters of the algorithm must be tuned in order to produce a relevant approximation of the original image. The evolution of the 2D CMLM in time is demonstrated in Fig. 7. The original image is depicted in Fig. 7(a); its dot-skeleton representation – in Fig. 7(b). The pattern produced after 50 time-forward iterations is shown in part c; 100, 150, 200, 240 and 300 time-forward iterations – in parts d, e, f, g and h respec-

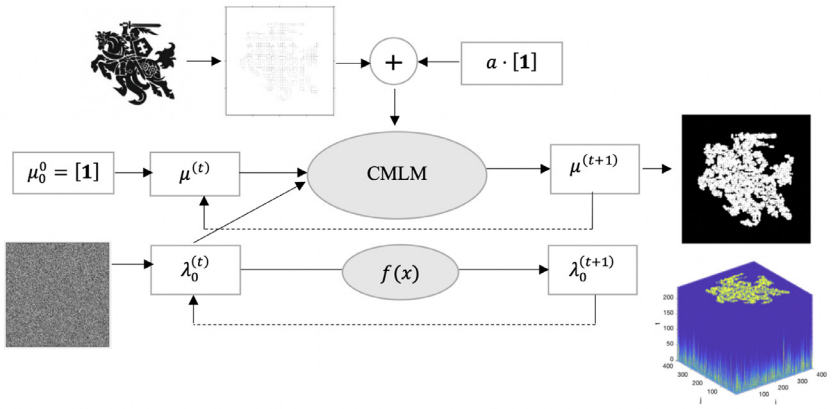

Fig. 6. The schematic diagram of the image communication algorithm ($\varepsilon = 0.13$; $\Delta a = 0.025$; the number of time-forward steps is 180).

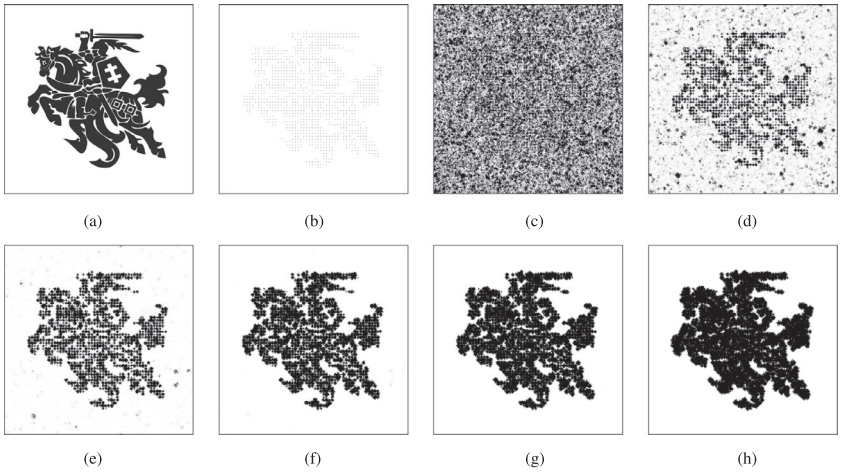

Fig. 7. The evolution of patterns produced by the 2D CMLM ($\varepsilon = 0.13$; $a = 3.565$; $\Delta a = 0.025$). The original image is shown in part (a); its dot-skeleton representation – in part (b) (the distance between adjacent pixels is five pixels). The inverse patterns produced after 50, 100, 150, 200, 240 and 300 time-forward iterations are shown in parts (c), (d), (e), (f), (g) and (h) respectively.

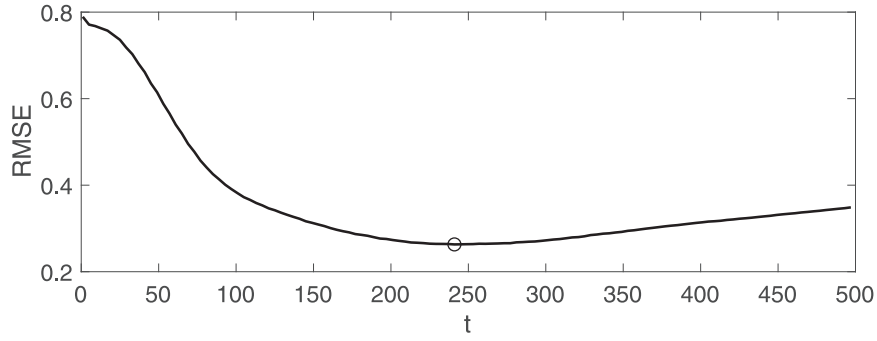

Fig. 8. The relationship between the RMSE and the number of time-forward iterations t. The RMSE is computed between the original secret image (Fig. 7 a) and the inverse pattern produced after the corresponding number of time-forward iterations. The x-axis represents the number of iterations, the y-axis represents the error. The minimum RMSE value for Fig. 7(a) is reached after 240 time-forward iterations.

tively. The best reconstruction of the original image (in terms of RMSE) is produced after 240 time-forward iterations (Fig. 8).

Security analysis is an integral part of any communication scheme. Security analysis of communication schemes based on self-organizing patterns has been thoroughly analyzed in [10]. The proposed scheme also belongs to the class of image hiding schemes based on self-organizing patterns – and the security issues of the proposed scheme are exactly the same. If, however, the security of the communication scheme needs to be strengthened – an additional steganographic layer can be introduced into the communication algorithm [14].

5. Concluding remarks

This paper presents an image hiding scheme based on the simplified nilpotent model of the 2D CMLM. The essential feature of this scheme is the ability to reveal the secret in a single image produced during the evolution of the 2D lattice. In other words, the scheme does not require computing a difference image between two patterns (one developed from the perturbed initial conditions, another – from the non-perturbed initial conditions).

It is important to observe that the proposed image hiding scheme is based on the effect of divergence in the 2D CMLM.

Therefore, the ability to interpret the pattern produced by the 2D CMLM depends on the cut-off value used to visualize the distribution of $\mu^{(t)}(i, j)$. In other words, the effect of divergence would prevent the interpretation of the secret image if only one would not know the pre-determined cut-off value. This is an additional security feature of the proposed scheme compared to similar image hiding schemes based on self-organizing patterns.

Every new scheme should be compared with the existing schemes. As mentioned previously, the proposed scheme cannot be compared with steganographic schemes. It is also completely different from any watermarking scheme. Comparisons between the presented scheme and any existing image hiding scheme based on self-organizing patterns is also not possible because the presented scheme does not require a difference image. Nevertheless, the presented scheme is compared to the automaton image hiding scheme.

The presented image hiding scheme could be employed in secure secret image communication algorithms – however this goes beyond the scope of this paper and remains a definite objective of future research.

Declaration of interests

The authors declare that they have no known competing financial interests or personal relationships that could have appeared to influence the work reported in this paper.

Acknowledgement

This research was supported by the Business Support Fund of Kaunas University of Technology (AlgebMIS).

References

[1] Chat H, Manneville P. Coupled map lattices as cellular automata. J Stat Phys 1989;56(3–4):357–70.
[2] Wang J, Li Y, Zhong S, Hou X. Analysis of bifurcation, chaos and pattern formation in a discrete time and space Gierer–Meinhardt system. Chaos Soliton Fract 2019;118:1–17.
[3] Huang T, Zhang H. Bifurcation, chaos and pattern formation in a space- and time-discrete predatorprey system. Chaos Soliton Fract 2016;91:92–107.
[4] MDS H, Martn JS. Travelling waves associated with saddle-node bifurcation in weakly coupled CML. Phys Lett A 2010;374(33):3292–6.
[5] Guangqing L, Smidtaite R, Navickas Z, Ragulskis M. The effect of explosive divergence in a coupled map lattice of matrices. Chaos Soliton Fract 2018;113:308–13.
[6] Gao Y, Zhang Q, Wang L, Feng L, Gao L, Zhang G, Xia C, Xin X. Highly fluorescent liquid-crystal based on biomolecule and dye self-assembly and their luminescence behavior in solvents for the detection of fe3+. Colloids Surf A 2018;546:276–84.
[7] Grafke T, Cates ME, Vanden-Eijnden E. Spatiotemporal self-organization of fluctuating bacterial colonies. Phys Rev Lett 2017;119(18):188003.
[8] Cherkashin AA, Vanag VK. Self-organization induced by self-assembly in microheterogeneous reaction-diffusion system. J Phys Chem B 2017;121(9):2127–31.
[9] Suzuki Y, Takayama T, Motoike IN, Asai T. Striped and spotted pattern generation on reactiondiffusion cellular automata – theory and LSI implementation. J Unconven Comput 2007;3(1):1–13.
[10] Saunoriene L, Ragulskis M. Secure steganographic communication algorithm based on self-organizing patterns. Phys Rev E 2011;84:056213.
[11] Ishimura K, Komuro K, Schmid A, Asai T, Motomura M. Image steganography based on reaction diffusion models toward hardware implementation. Nonlinear Theory Appl IEICE 2014;5(4):456–65.
[12] Vaidelys M, Ragulskiene J, Ziaukas P, Ragulskis M. Image hiding scheme based on the atrial fibrillation model. Appl Sci 2015;5:1980–91.
[13] Ziaukas P, Ragulskis T, Ragulskis M. Communication scheme based on evolutionary spatial games. Physica A 2014;403:177–88.
[14] Vaidelys M, Ziaukas P, Ragulskis M. Competitively coupled maps for hiding secret visual information. Physica A 2016;443:91–7.
[15] Vaidelys M, Lu C, Cheng Y, Ragulskis M. Digital image communication scheme based on the breakup of spiral waves. Physica A 2017;467:1–10.
[16] Moffitt JR, Macdonald P, Lindne JF. Self-erasing perturbations of Abelian sandpiles. Phys Rev E 2004;70(1):016203.
[17] Wolpert DH. Ubiquity symposium: evolutionary computation and the processes of life: what the no free lunch theorems really mean: how to improve search algorithms. Ubiquity 2013;2(1–2):15.
[18] Kaneko K. Spatiotemporal chaos in one and two-dimensional coupled map lattices. Physica D 1989;37:60–82.
[19] May R. Simple mathematical models with very complicated dynamics. Nature 1976;261(5560):459–67.
[20] Atay FM, Biyikoglu T, Jost J. Network synchronization: spectral versus statistical properties. Physica D 2006;224(1–2):35–41.
[21] Kaneko K. From globally coupled maps to complex-systems biology. Chaos 2015;25:097608.
[22] Gravner J, Johnson K. Coupled map lattices as musical instruments. Comput Music J 2018;42(2):22–34.
[23] Nematzadeh H, Enayatifar R, Motameni H, Guimares FG, Coelho VN. Medical image encryption using a hybrid model of modified genetic algorithm and coupled map lattices. Opt Lasers Eng 2018;110:24–32.
[24] Sam IS, Devaraj P, Bhuvaneswaran RS. An intertwining chaotic maps based image encryption scheme. Nonlinear Dynam 2012;69(4):1995–2007.
[25] Wang X, Luan D. A novel image encryption algorithm using chaos and reversible cellular automata. Commun Nonlinear Sci Numer Simul 2013;18(11):3075–85.